crystals

MDPI

*Article*

# The Fabrication of Gold–Silver Bimetallic Colloids by Microplasma: A Worthwhile Strategy for Counteracting the Surface Activity of Avian Influenza Virus

**Muhammad Zubair [1,*], Muhammad Shahid Rafique [1], Afshan Khalid [1], Tahir Yaqub [2], Muhammad Furqan Shahid [2,3], Suliman Yousef Alomar [4] and Muhammad Ali Shar [5]**

[1] Department of Physics, University of Engineering and Technology, Lahore 54890, Pakistan
[2] Institute of Microbiology, University of Veterinary and Animal Sciences, Lahore 54590, Pakistan
[3] Veterinary Research Institute, Lahore 54000, Pakistan
[4] Zoology Department, College of Science, King Saud University, Riyadh 11451, Saudi Arabia
[5] Department of Mechanical& Energy Systems Engineering, Faculty of Engineering and Informatics, University of Bradford, Bradford BD7 1DP, UK
* Correspondence: zubairdarsana1511@gmail.com

**Abstract:** In the present project, fructose-stabilized gold, silver and gold–silver bimetallic colloids have been synthesized by the electrochemical reduction of $HAuCl_4 \cdot 3H_2O$ (Au precursor) and $AgNO_3$ (Ag precursor), employing the atmospheric pressure microplasma technique. X-Ray Diffraction patterns of gold–silver bimetallic particles exhibit (111), (200) and (220) planes identical to gold and silver NPs depicting FCC structures. The decrease in the peak intensities of Au–Ag (111) and Au–Ag (200) as compared to those of Au (111) and (200) is due to the formation of Au–Ag alloys. The FE-SEM image of gold–silver bimetallic NPs has revealed an adequate change in morphology as compared to the morphology of gold NPs and silver NPs. The majority of the gold–silver bimetallic NPs are spherical and are uniformly dispersed. The EDS spectra of (Au–Ag) confirm the presence of metallic gold and silver. The appearance of a single Surface Plasmon Resonance (SPR) peak in the UV–VIS absorption spectra of gold–silver colloids and its position in between the SPR peaks of the UV–VIS absorption spectra of gold and silver colloids justify the formation of gold–silver bimetallic alloy particles. In DLS measurements, the size distribution of gold–silver bimetallic colloids carries a narrow range 55 to 117 nm as compared to the size distribution of gold and silver colloids. The compatibility of the sizes of these colloids and the influenza virus belonging to the Orthomyxoviruses family (size range 80–300 nm with different morphologies) are assumed to stand responsible for an effective bio-conjunction with Influenza viruses. Au–Ag bimetallic nanostructures have synergistically improved their antiviral activity against H9N2 influenza virus as compared to monometallic AuNPs and AgNPs. Thus, the Au–Ag nanostructured alliance has been proven to be more effective and is capable of manifesting high antiviral efficacy.

**Keywords:** microplasma fabrication; bimetallic colloids; nanostructures; analytical techniques; antiviral activity; synergy



**Citation:** Zubair, M.; Rafique, M.S.; Khalid, A.; Yaqub, T.; Shahid, M.F.; Alomar, S.Y.; Shar, M.A. The Fabrication of Gold–Silver Bimetallic Colloids by Microplasma: A Worthwhile Strategy for Counteracting the Surface Activity of Avian Influenza Virus. *Crystals* **2023**, *13*, 340. https://doi.org/10.3390/cryst13020340

Academic Editors: Mohamed A. Tahoon and Abdelfattah Amari

Received: 21 January 2023
Revised: 10 February 2023
Accepted: 13 February 2023
Published: 16 February 2023



## 1. Introduction

The influenza virus is a consistent global fear and threat with the potential to cause pandemics worldwide in humans and animals [1]. The Avian Influenza Virus H9N2 belonging to the orthomyxoviridae family was initially isolated from China poultry forms. It had resulted in large-scale economic losses due to the decreased egg production and the increased mortality of chicks in the past [2]. The H9N2 virus has also been a source of sporadic infections in humans in Asia since 1998 [3]. The concerns about its pandemic potentials have been pressing researchers to recognize and sort alternative anti-influenza agents. However, the evolution of various virus strains and the emergence of their antiviral

drug resistance has put a huge burden on controlling influenza [4]. For the survival of human and animal lives, there is an utter need to develop new treatment strategies for combatting influenza virus activities. Metallic nanocomposites have a great potential to fight against viruses and to be an effective alternative to conventional antiviral drugs, particularly against influenza. Recent developments in the field of nanoscience and nanotechnology have entirely altered the pattern of human and animal life [5]. As the nexus of nanotechnology in the medical field is developing more and more, the use of nanostructures in the creation of novel and efficient medical diagnostics and therapies is becoming a growing strategy [6].

In previous research, metal nanoparticles including Ag, Au, Cu, Pt and metal oxides of Fe, Zn, Cu and Ti have been explored extensively and have earned tremendous popularity as antimicrobial agents [7–9]. Among the metallic nanoparticles, both silver and gold nanoparticles have been demonstrated to exert antimicrobial effects against a wide range of pathogens such as parasites, fungi, bacteria and viruses [10,11]. As antiviral agents, both AuNPs and AgNPs in monometallic forms have been investigated against various viral diseases, particularly against influenza virus. In one of the past studies, influenza virus activity was effectively inhibited by anionic AuNPs [12]. In another past investigation, the inhibitory effects of AgNPs against influenza virus activity were assessed in a Hemagglutination Assay (HA) [13]. Recently, J. Kim and co-workers reported a strong antiviral activity of porous AuNPs on the H1N1 and H9N2 influenza virus strains in HA protocol using MDCK cells as a culture medium [14]. In addition, Chang et al. synthesized the Ag and Au nanoparticles and observed a reduction in the cytopathic effect induced by human and avian influenza viruses. They also reported that TPNT1 was very effective in blocking the viral entry and, thus, preventing viral infection [15]. Similarly, Bhattacharya and Jagirdar studied the core shell formulism of Ag and Au nanoparticles. In this study, Au was used as a core and Ag was used as a shell, and the details of the underlying mechanism were presented [16].

In addition, TPNT1 also effectively reduced the cytopathic effects induced by human (H1N1) and avian (H5N1) influenza viruses, including the wild-type and oseltamivir-resistant virus isolates. Together with the previously demonstrated efficacy as antimicrobials, TPNT1 can block viral entry and inhibit or prevent viral infection to provide prophylactic effects against both SARS-CoV-2 and opportunistic infections.

From previous research, silver NPs have been found to be more effective as an antibacterial agent as compared to gold NPs. On the other hand, in most of the studies, gold NPs have been seen as less toxic and more biocompatible than AgNPs [11,17]. Their combination in the form of a nano-alloy and core-shell has received massive attention in exploring their antimicrobial potentials [18]. For example, silver-gold colloids in alloy form fabricated by the chemical co-reduction method have demonstrated a strong antibacterial effect [19,20]. An improved efficiency of Au–Ag bimetallic colloids fabricated by the chemical method has been studied in the past [21]. In other similar research, an enhanced antibacterial efficacy of Au–Ag core-shell NPs synthesized via the chemical route has been observed [22]. Likewise, the antibacterial activity of bio-synthesized (Au–Ag) NPs was studied by Ramasamy and coworkers [23]. A promising synergy in the antibacterial efficiencies of bimetallic NPs (Ag–Cu) as compared to their monometallic counterparts has also been reported [24,25]. More recently, Diana Lomelí-Marroquín and co-workers fabricated (Au–Ag) bimetallic nanoparticles in the one-pot green synthesis, using starch as a reducing and capping agent, and studied their antimicrobial and anticancer activity [26].

From the brief literature survey, it is seen that Au–Ag bimetallic NPs fabricated by various synthesis roots have been mostly deployed in examining their antibacterial tendencies against various pathogens. There is limited literature available regarding the antiviral record of bimetallic nanoparticles, particularly against the influenza viruses. Most recently, our group has examined the antiviral capability of gold–PVP nanocomposites against the avian influenza virus strain H9N2. In these investigations, gold–PVP nanocomposites have shown an enhanced antiviral activity as compared to gold NPs alone [27].

The present research work is about the fabrication of gold, silver and gold–silver bimetallic nanoparticles by the atmospheric pressure microplasma technique and about testing their antiviral activities against avian influenza virus. To the best of our knowledge, no such research activity was found in the past. In microplasma-assisted fabrication, the nanoparticles are synthesized by the reduction of their respective precursors in an aqueous medium without using a chemical reducing agent [28]. The size and morphology of nanoparticles are the important parameters in biomedical applications, and they are tuned by controlling the experimental parameters. These include the microplasma discharge time, the gas flow rate and the concentration of precursor salt [29].

## 2. Materials and Methods

### *2.1. Materials*

Hydrogen tetrachloroaurate(III) trihydrate $HAuCl_4 \cdot 3H_2O$ (Merck) (393.83 g/mole) has been used as a gold precursor. Analytical grade 169.87 g/mol silver nitrate $AgNO_3$ (Sigma Aldrich) has been used as a silver precursor. D-Fructose 180.16 g/mol (Avonchem UK) has been used as a stabilizer. Distilled water has been used as a solvent. All of these were purchased from the local market. A home-designed atmospheric pressure microplasma setup was used as the electrochemical reducing technique.

#### 2.1.1. Preparation of Stock Solutions

A 100 mL stock solution of $AgNO_3$ with a concentration of 10.0 mM was prepared by dissolving 0.169 g of $AgNO_3$ in 100 mL of distilled water. A 100 mL stock solution of $HAuCl_4 \cdot 3H_2O$ with a concentration of 25.0 mM was prepared by dissolving 1.00 g of hydrogen tetrachloroaurate(III) trihydrate $HAuCl_4 \cdot 3H_2O$ in 100 mL of distilled water. The solutions were separately stirred magnetically for 25 min to ensure the homogeneity.

#### 2.1.2. Preparation of 0.25 mM Gold Precursor

A total of 1.0 mL of 25.0 mM stock solution of gold (III) chloride trihydrate/chloroauric acid ($HAuCl_4 \cdot 3H_2O$) and 0.049 g of D-Fructose was added to 99.0 mL of distilled water. The whole solution was magnetically stirred for 20 min to produce homogeneous solution with 0.25 mM gold precursor and 2.5 mM D-Fructose.

#### 2.1.3. Preparation of 0.5 mM Gold Precursor

A total of 2.0 mL of 25.0 mM stock solution of gold (III) chloride trihydrate/chloroauric acid ($HAuCl_4 \cdot 3H_2O$) and 0.089 g D-Fructose was added to 98.0 mL of distilled water. The whole solution was magnetically stirred for 20 min to produce a homogeneous solution with 0.50 mM gold precursor and 5.0 mM D-Fructose.

#### 2.1.4. Preparation of 0.25 mM Silver Precursor

A total of 2.5 mL of 10.0 mM stock solution of $AgNO_3$ and 0.049 g was added to 97.5 mL of distilled water. The whole solution was stirred magnetically for 20 min to prepare a homogeneous 0.25 mM silver precursor with 2.5 mM D-Fructose

#### 2.1.5. Preparation of 0.50 mM Silver Precursor

A total of 5.0 mL of 10.0 mM stock solution of $AgNO_3$ and 0.089 g was added to 95.0 mL of distilled water. The whole solution was stirred magnetically for 20 min to prepare a homogeneous 0.50 mM silver precursor with 5.0 mM D-Fructose.

### *2.2. Fabrication of Nanostructured Materials by Atmospheric Pressure Microplasma*

In our research work, we used a home-designed atmospheric pressure microplasma facility, as shown in Figure 1, to execute the synthesis of metal colloids through plasma–liquid interactions. The microplasma was produced by applying a high dc voltage up to 5–6 kV (power supply output 30 KV, 66 mA Glassman high voltage, INC) between a cathode and an anode. The stainless-steel capillary with an internal diameter of 0.28 mm

and a wall thickness of 0.145 mm acted as cathode, and a carbon rod that was 4 cm in length and 8.0 mm in diameter was dipped in the precursor solution as an anode. Microplasma discharge was produced in argon gas flowing through the capillary with a constant flow rate of 35 Sccm. The distance between the precursor solution and capillary needle was kept at 2 mm, while the distance between the anode and cathode was 3 cm. At the surface of the precursor solution, the microplasma discharge acted as a cathode, while the graphite rod immersed in the precursor cell served as an anode. A non-thermal stable glow-like microplasma discharge consists of high-energy species electrons, ions, UV radiations and neutral and reactive radicals. The microplasma–precursor aqueous solution interface becomes the active reaction zone. The cathodic microplasma discharge impinges on the anodic metal precursor–aqueous solution. The electrochemical catalysis reduces the metal cations that interact with the micro plasma-donated electrons to form metal atoms. The metal atoms come close by van der Waals forces. They nucleate and aggregate to form metal nanoparticles [30]. The underlying basic idea for the synthesis of metallic nanostructures using plasma, represented by Equation (1), has been reported in most of the research papers [31,32].

$$\text{Metal}_{(\text{cation})} + \text{ne}_{(\text{microplasma})} \text{ ———— } \text{M}^{\text{o}}{}_{(\text{atom})} \quad (1)$$

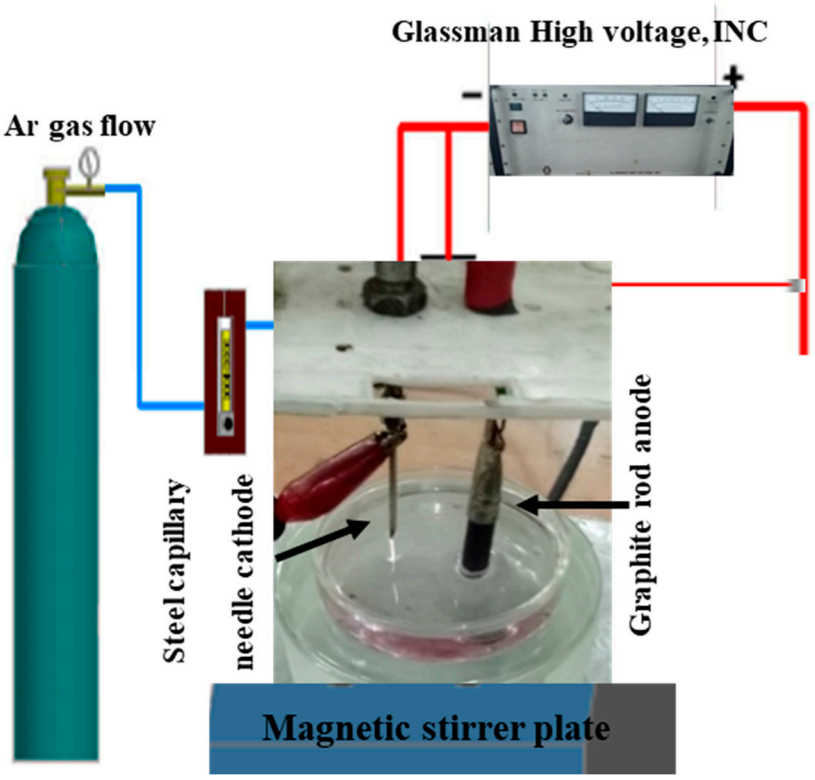


**Figure 1.** Atmospheric Pressure Microplasma Setup for the Fabrication of Metallic Colloids.

Figure 1 illustrates the atmospheric pressure microplasma setup for fabricating nanostructures. Figure 2 is a block diagram of the roadmap for the synthesis of metal colloids through microplasma electrochemical reduction.

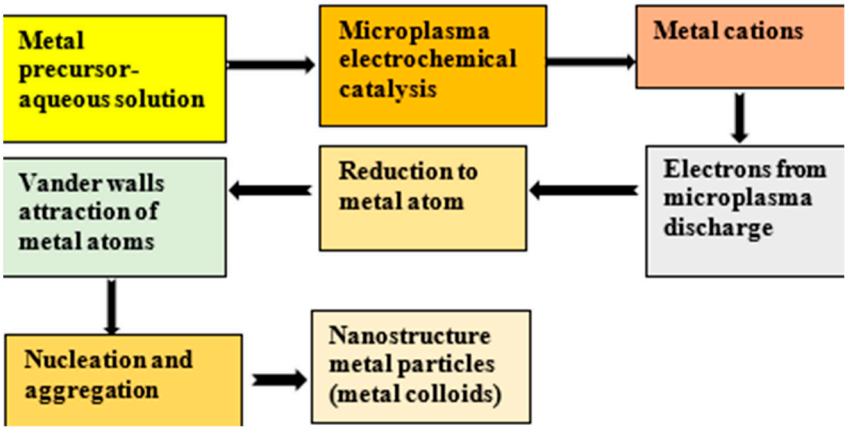


**Figure 2.** Block diagram demonstrating the bottom-up approach to produce nanoparticles by microplasma.

2.2.1. Synthesis of Gold Colloids

Figure 2 shows a reaction cell with a volume of 100 mL containing hydrogen tetrachloroaurate(III) trihydrate $HAuCl_4 \cdot 3H_2O$ (0.5 mM composition) as a precursor solution, which was exposed to atmospheric pressure microplasma for 10 min. The microplasma discharge is the source of electrons among other microplasma species. Gold cations, after the electrochemical reduction, interact with microplasma-produced electrons to form gold atoms, followed by limited agglomeration to produce gold nanostructure particles. After 2–3 min of plasma exposure time, the color of the solution was changed from yellow to purplish, showing the first visual indication of gold colloids formation, as shown in Figure 3a, represented by $(Au\text{-}10)_{0.5}$.

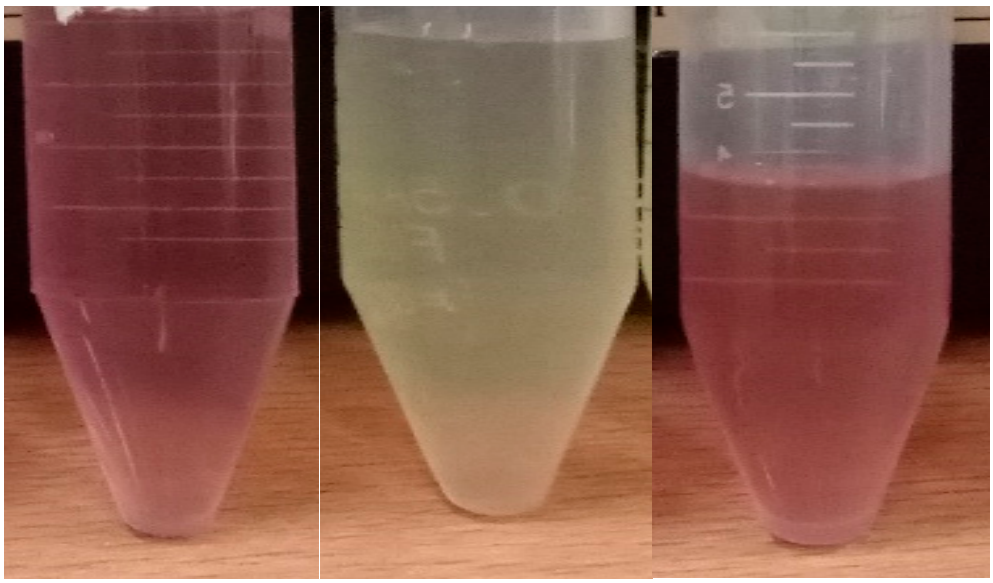

(**a**) (**b**) (**c**)

**Figure 3.** Microplasma-assisted synthesis of (**a**) $(Au\text{-}10)_{0.50}$, (**b**) $(Ag\text{-}10)_{0.50}$ and (**c**) $(Au–Ag\text{-}10)_{0.50}$.

2.2.2. Synthesis of Silver Nanoparticles

A reaction cell containing 100.0 mL of the $AgNO_3$ precursor with a concentration of 0.50 mM was exposed to atmospheric pressure microplasma for 10 min. Silver cations, after the electrochemical reduction, interact with microplasma-produced electrons to form silver atoms, followed by agglomeration to produce silver nanostructured particles. After 2–3 min of plasma exposure time, a colorless transparent solution of $AgNO_3$ precursor was changed from a yellowish one, showing the first visual indication of silver colloids formation, as shown in Figure 3b, represented by $(Ag\text{-}10)_{0.5}$.

#### 2.2.3. Synthesis of Gold–Silver Bimetallic Colloids

A Volume of 50 mL with concentration 0.25 mM of $HAuCl_4 \cdot 3H_2O$ precursor solution was added to a volume of 50 mL $AgNO_3$, precursor solution with concentration 0.25 mM The whole solution was mixed and stirred magnetically for 20 min. The solution was initially colorless. The microplasma was energized by a high dc voltage of 5 kV between the stainless-steel capillary (through which argon gas flows at a rate of 35 Sccm) and the carbon rod dipped in the precursor. The current was maintained from 2 to 2.5 mA. With the exposure of microplasma discharge for 10 min, a light reddish color appeared initially, followed by the appearance of a pinkish mixed precursor. These observations suggest that AuNPs formed first at the early stage of (Au–Ag) colloids. Then, with time, they turn pinkish, indicating the contribution of AgNPs in (Au–Ag) bimetallic colloids, named (Au–Ag)-10), as shown in Figure 3c, represented by $(Au–Ag\text{-}10)_{0.50}$.

### *2.3. Investigation of the Antiviral Activities of Gold and Silver Nanostructures*

Investigations of the antiviral tendencies of gold, silver and gold–silver bimetallic nanostructures have been carried out by adopting inoculation, the harvesting of chorioallantoic fluid and the Hemagglutination Assay (HA) protocol. An equal volume of gold, silver, and gold-silver colloids were separately mixed with equal volume of confirmed Avian Influenza Virus AIV (H9N2) of $10^6$ $EID_{50}$ were mixed in a microfuge tube. AIV (H9N2) of $10^6$ $EID_{50}$ was procured from the Influenza Lab, Institute of Microbiology, the University of Veterinary and Animal Sciences, Lahore. The virus and nanoparticles were incubated at 37 °C for 30 min in an incubator so that the nanoparticles could react.

#### 2.3.1. Inoculation in Embryonated Chicken Eggs

A total of about 0.2 mL of the inoculum was inoculated in 9-day-old embryonated chicken eggs via the Chorio-Allantoic Sac (CAS) route by using sterile disposable syringes. After the inoculation, the drilled eggshell was sealed by using wax, as shown in Figure 4a. After the inoculation, the eggs were incubated at 37 °C for 48 h for the propagation of the virus.

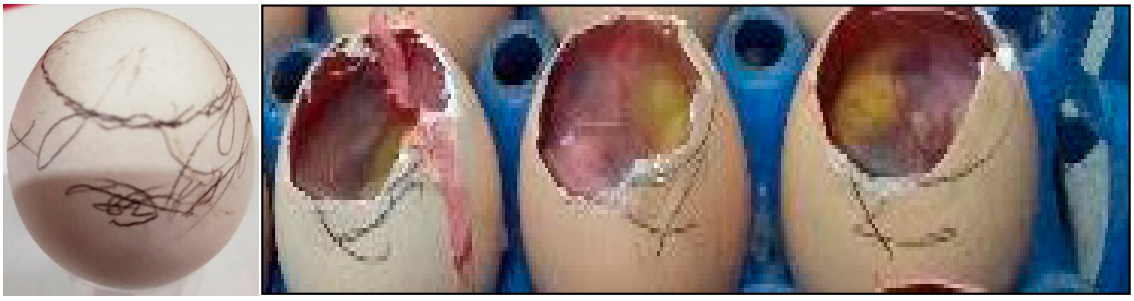

(**a**) (**b**)

**Figure 4.** (**a**) Virus, nanoparticles inoculation; (**b**) Fluid harvesting of Chorio-Allantoic Fluid (CAF).

#### 2.3.2. Fluid Harvesting

The embryonated chicken eggs were chilled overnight at 4 °C. After proper chilling, the eggs were placed in a Level II bio-safety cabinet and were disinfected with 70% ethanol. Over the air sac, the eggshell portion was removed using sterile, sharp scissors. The air sac membrane was removed. With the help of sterile forceps, the head of the embryo was gently pressed, and Chorio-Allantoic Fluid (CAF) was picked up by using a 5 mL disposable syringe, as shown in Figure 4b. The pooled CAF was separated in properly labeled 15 mL falcon tubes.

2.3.3. Hemagglutination Test (HA)

The chorio-allontioc fluid (CAF) harvested from the embryonated chicken eggs was checked for hemagglutination activity via the hemagglutination test (HA). This test was carried out according to the procedure referenced by Alexander and Chettle (Alexander and Chettle 1977). For this procedure, 50 µL of normal saline (NS) was dispensed in all the wells of the micro titration plate by using a multi-channel micro pipette. Then, 50 µL of the harvested CAF was dispensed in the first well. After that, twofold serial dilutions of the CAF were made from 1:2 to 1:2048. This was accomplished by transferring 50 µL into the next wells, and so on, up to the 11th well. After this step, 50 µL of 1% RBCs suspension was dispensed into all of the wells. The 12th well was kept as the negative control or RBCs control, which contains only 1% RBCs suspension and normal saline. After that, the micro titration plate was incubated at 37 °C for 20–30 min. The results were recorded after the incubation when RBCs in the 12th well were completely settled down to form a clearly visible bead at the bottom of the well. The HA test observations were performed in triplicate to ensure quality results. The HA activity being negative means that the virus is disabled or neutral, and the HA activity being positive confirms the presence of the virus. The virus has a tendency to adhere to the surface of red blood cells and cause agglutination, preventing them from settling at the bottom of a well and not letting them to form a bead. This is called positive HA activity, as shown in the micro-titer plates Figure 5.


**Figure 5.** HA activity of H9N2 after the interaction with nanostructured particles.

*2.4. Characterization Techniques*

To assess the functional aspects of fabricated products, analytical techniques have been executed to characterize gold, silver and gold–silver nanostructures. The formation of their colloids was primarily experienced through visual observations. The crystallinity, phases and planes of the nanostructured materials (gold, silver and gold–silver NPs/NCs) have been probed with Bruker $D_8$ DISCOVER Advance in Bragg–Brentano mode with Cu Kα radiation (40 KV, 1.54 A and 40 mA). The morphology of the gold and silver nanostructures was investigated with a Nova Nano SEM 450 Field-Emission Scanning Electron Microscope (FE-SEM). The compositional analysis of the nanostructured materials was carried out by energy dispersive X-ray spectroscopy (EDS) attached with the FE-SEM. UV–VIS spectroscopic studies of gold and silver nanostructures and their nanostructured composites were accomplished by using Agilent Technologies Cary 60, ranging from 200 to 800 nm, with a resolution of 1 nm. The dynamic light scattering technique, with a standard He-Ne laser (632.8 nm) used as a light source (BI-200SM, Brookhaven Instrument Corp.), has been used to characterize the hydrodynamic size distributions of the colloidal dispersions.

## 3. Results and Discussion

*3.1. X-ray Diffrectometry*

X-ray diffraction analyses of all the samples were carried out to confirm the phase and crystalline nature of the gold, silver and gold–silver bimetallic nanoparticles prepared by drop-casting the colloids separately on glass strips, followed by drying at room temperature. Figure 6 shows the X-ray diffractograms of all of the prepared samples 2θ ranging from

20° to 75°. The identical Bragg's reflections of (Au-10), (Ag-10) and (Au–Ag-10) appearing at 2θ = 38.2°, 44.4° and 64.58° correspond to (111), (200) and (220) planes, respectively, and are indexed as face-centered cubic (FCC) structures [18,33]. The peaks of Ag were recognized by matching this diffraction pattern with the reference card #00-001-1167, which ensured the formation of a cubic crystal structure of Ag with lattice parameters of 4.08 Å. Similarly, the peaks of Au were confirmed by matching its peaks with the reference card #00-001-1172 with lattice parameters of 4.0699 Å. An additional peak of (AgO) has been observed due to the rapid oxidation of silver nanoparticles [34] and the same in the bimetallic Ag–Au-10 nanoparticles. This peak of Ag–O was identified by the reference card #00-022-0472.

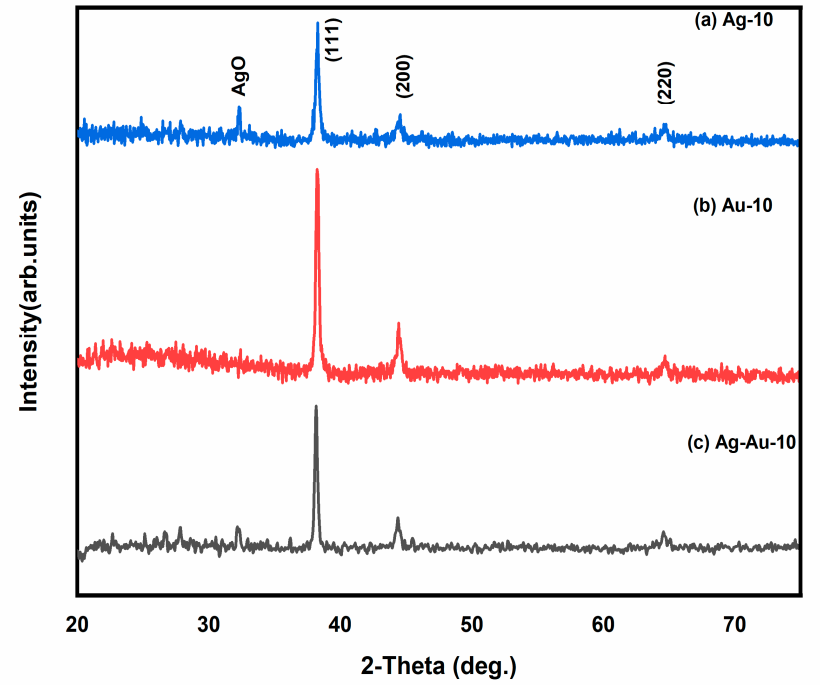


**Figure 6.** XRD patterns of (**a**) Ag-10, (**b**) Au-10 and (**c**) Au–Ag-10 nanoparticles.

These identical Bragg's reflections of AuNPs, AgNPs and 'Au–Ag' NPs are due to the almost similar interplanner distances of both Au (0.408) and Ag (0.409), supporting the mixable trend of Au and Ag atoms in a nanoparticle structure, as evidenced in previous investigations [35,36]. The peak intensities of Au (111) and Au (200) are higher in comparison to those of Ag (111) and Ag (200). However, there is a slight decrease in the peak intensities of Au–Ag (111) and Au–Ag (200) as compared to those of Au (111) and (200). It appears that this decrease in the peak intensities of Au–Ag is due to the formation of Au–Ag alloys [34,37]. In addition, the crystallite size was calculated using Scherer's formula, which was found to be 35 nm and 29 nm for Au and Ag nanoparticles and 30 nm for their composite [38].

### *3.2. Field-Emission Scanning Electron Microscope (Fe-Sem) Analyses*

#### 3.2.1. SEM of $(Au\text{-}10)_{0.50}$

Figure 7a shows the FE-SEM image of $(Au\text{-}10)_{0.50}$. The picture demonstrates that the gold NPs are maximum in spherical shape and are not uniformly dispersed. Recently, identical FE-SEM images of gold nanoparticles prepared by the green synthesis technique have been reported [39]. Gold nanoparticles synthesized by the green method at room temperature, where the majority of the particles seem spherical, have also been reported in the near past [40].

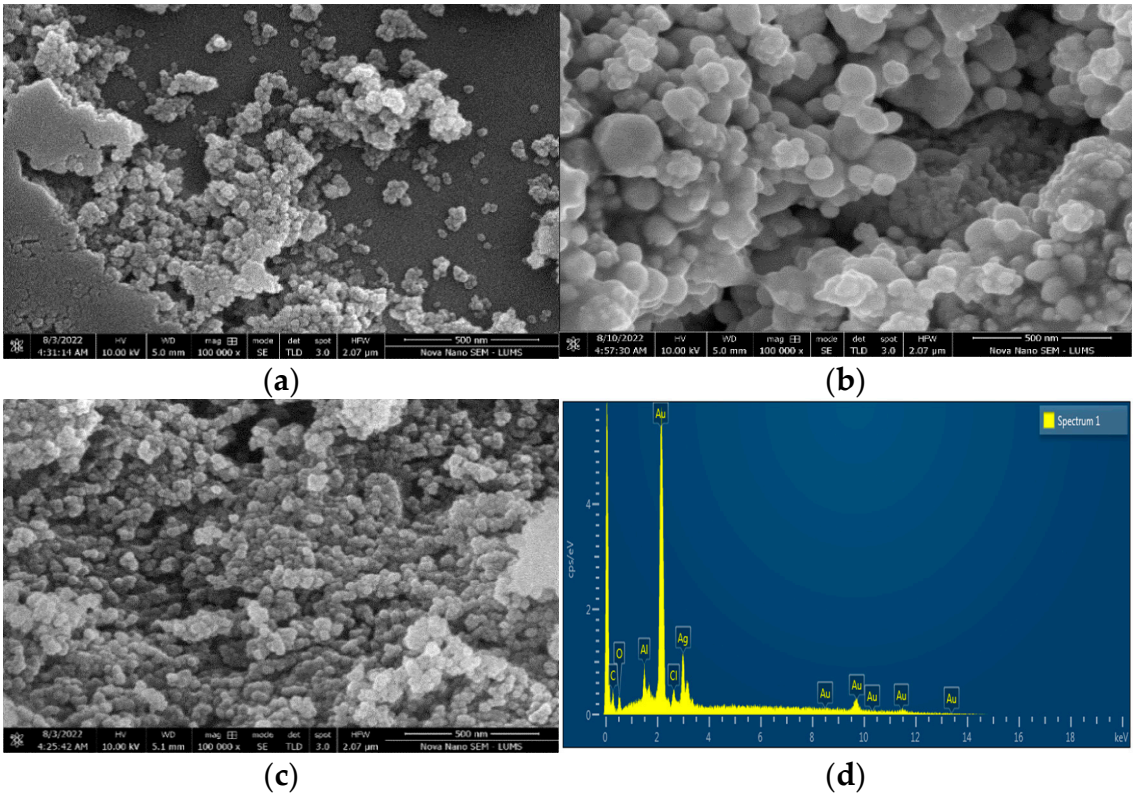


**Figure 7.** FE-SEM images of (**a**) Au-10, (**b**) Ag-10, (**c**) Au–Ag-10 and (**d**) EDX of Au–Ag-10.

#### 3.2.2. SEM of $(Ag\text{-}10)_{0.50}$

Figure 7b is the FE-SEM image of $(Ag\text{-}10)_{0.50}$, showing uniform dispersions. The morphological studies suggest that maximum particles are in a spherical shape. These observations are inconsistent with recent findings based upon the FE-SEM analysis of silver NPs fabricated by green synthesis [41]. In one of the previous investigations, the silver nanoparticles were synthesized by the reduction in the silver precursor ($AgNO_3$) of a concentration of 1.0 mM by 25 min of atmospheric pressure microplasma discharge. The SEM images of these silver nanostructures revealed spherical cum multi-shaped nanoparticles [42].

#### 3.2.3. SEM of $(Au–Ag)_{0.50}$ Bimetallic Nanoparticles

The FE-SEM image of gold–silver bimetallic NPs reveals an adequate change in morphology as compared to the morphology of fructose-stabilized gold particles. The majority of the Au–Ag composite particles are spherical and are uniformly dispersed, as shown in Figure 7c. It appears that silver nanoparticles have influenced the morphology of Au–Ag composites. The change in the morphology of Au–Ag was also reflected in the XRD analyses of Au–Ag bimetallic nanocomposites. The decrease in the peak intensities of Au–Ag (111) and Au–Ag (200), as compared to those of Au (111) and (200), as shown in Figure 6, is due to the formation of Au–Ag alloys [37]. A similar kind of change in the morphology of bimetallic gold–silver nanoparticles produced by one-step synthesis has also been observed in previous activity [43,44]. In another previous research activity, the FE-SEM images of bimetallic noble metal nanostructures showed multiple shapes depending upon the ratio of constituents [45]. The EDX spectrum of (Au–Ag) confirms the presence of metallic gold and silver masked by C and O peaks as the major constituents of D-Fructose, as shown in Figure 7d. The weight percentage of all the involved elements is provided in Table 1.

**Table 1.** Weight percentage of all the involved elements.

| Elements | Ag | Au | C | O | Cl |
|---|---|---|---|---|---|
| Wt% | 20.51 | 68.36 | 4.98 | 4.49 | 1.66 |

### *3.3. UV—Visible Spectroscopic Analyses*

The UV–VIS spectra of fructose-stabilized $(Au\text{-}10)_{0.5}$, $(Ag\text{-}10)_{0.5}$ and $(Au–Ag\text{-}10)_{0.5}$ colloids are shown in Figure 8a–c, respectively.

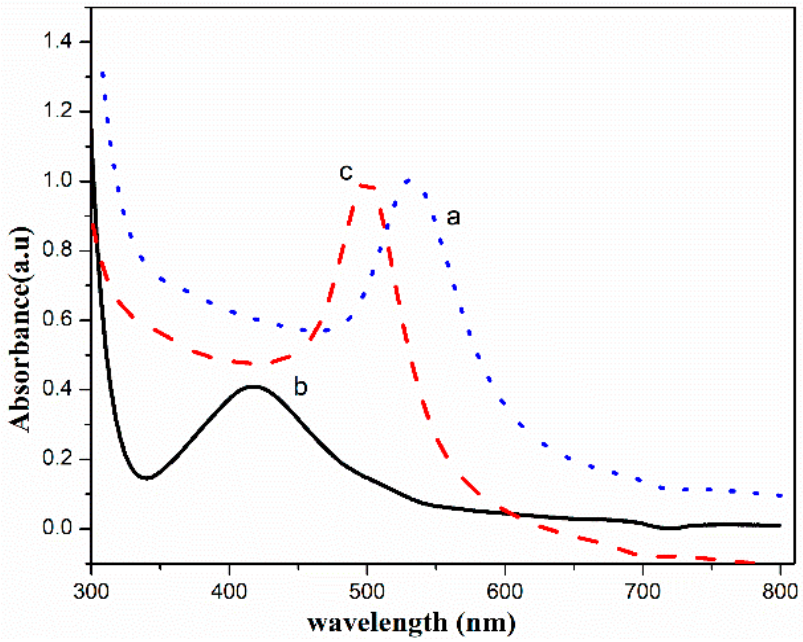


**Figure 8.** UV–VIS spectra of fructose-stabilized (**a**) $(Au\text{-}10)_{0.5}$, (**b**) $(Ag\text{-}10)_{0.5}$ and (**c**) $(Au–Ag\text{-}10)_{0.5}$.

The surface plasmon resonance (SPR) of $(Au\text{-}10)_{0.5}$ and $(Ag\text{-}10)_{0.5}$ was observed at 532 nm and 410 nm, respectively. The maximum absorbance due to the surface plasmon resonance of the $(Au–Ag\text{-}10)_{0.5}$ nanoparticles was observed at 498 nm. The position of SPR in the case of $(Au–Ag\text{-}10)_{0.5}$ lying between the SPRs of $(Ag\text{-}10)_{0.5}$ and $(Au\text{-}10)_{0.5}$ justifies the formation of Au–Ag bimetallic NPs [46]. Furthermore, the position of SPR in the case of $(Au–Ag\text{-}10)_{0.5}$ was blue-shifted as compared to that of Au-10 NPs, suggesting a decrease in size in the bimetallic form as compared to Au-10 NPs [47]. The further appearance of a single SPR in $(Au–Ag\text{-}10)_{0.5}$ NPs confirms the formation of a gold–silver nano-alloy [48]. This is in agreement with the previous work, where the location of the SPR in Au/Ag NPs was found to be at 443 nm, lying intermediately between the SPR of AuNPs at 545 nm and that of AgNPs at 413 nm [39]. For core-shell structure, two peaks have been observed in the UV–VIS spectra seen in previous studies [22].

### *3.4. Dynamic Light Scattering Analyses*

#### 3.4.1. Size Distribution of $(Au\text{-}10)_{0.50}$

The size distributions of the gold colloids $(Au\text{-}10)_{0.50}$ are shown in Figure 9a. The hydrodynamic size of $(Au\text{-}10)_{0.50}$ consists of two distributions. Their size ranges from 12 nm to 149 nm, with 14 nm and 91 nm maximum intensities in the respective distributions. In one of the previous studies, the same approach was used to estimate the hydrodynamic size of the gold nanoparticles. In these investigations, the major particles size distribution peak at an average diameter of 75 nm was observed, while a small size distribution exhibited a particles size peak around 5–6 nm [49].

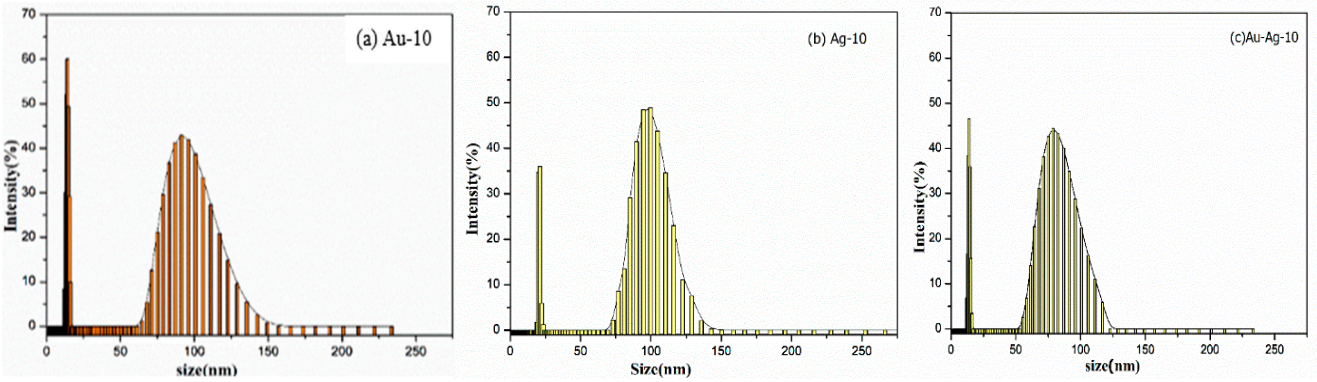


**Figure 9.** The particle size distribution of (**a**) gold $(Au\text{-}10)_{0.50}$ colloids, (**b**) silver $(Ag\text{-}10)_{0.50}$ and (**c**) gold–silver $(Au–Ag\text{-}10)_{5.0}$ bimetallic colloids.

#### 3.4.2. Size Distribution of $(Ag\text{-}10)_{0.50}$

The hydrodynamic size of $(Ag\text{-}10)_{0.50}$ consists of two distributions, as shown in Figure 9b. Their size ranges from 19 nm to 143 nm, with 21 nm and 99 nm maximum intensities in the respective distributions. In a past investigation, the size distribution of silver colloids produced by the chemical reduction method with an intensity-weighted technique has been reported. The major particles size distribution ranged from 60 to 100 nm, with the peak at an average diameter of 80 nm [42].

#### 3.4.3. Size Distribution of Gold–Silver $(Au–Ag\text{-}10)_{0.50}$

The hydrodynamic size of gold–silver bimetallic colloids $(Au–Ag\text{-}10)_{0.50}$ also consists of two distributions, as shown in Figure 9c. Their size ranges from 12 nm to 117 nm, with 16 nm and 78 nm maximum intensities in the respective distributions.

In summary, it is observed that the first distributions in $(Au\text{-}10)_{0.50}$, $(Ag\text{-}10)_{0.50}$ and $(Au–Ag\text{-}10)_{0.50}$ colloids produced by a microplasma discharge of 10 min lie within an identical range of (12–23 nm), regardless of the nature of the nanoparticle and the concentration of the precursor. The second distribution in the spectrum consists of a comparatively larger-sized range, i.e., 64–142 nm for $(Au\text{-}10)_{0.50}$, 70–143 nm for $(Ag\text{-}10)_{0.50}$ and 55–117 nm for $(Au–Ag\text{-}10)_{0.50}$. It can be interpreted that the narrow distribution of the small-sized range is independent of the nature of the particles. It is suggested that these narrow distributions could be due to the scattering of the laser due to the presence of some impurities in the samples [46]. However, the size distribution of gold–silver bimetallic colloids ($(Au–Ag\text{-}10)_{0.50}$) carries a narrow range of 55–117 nm as compared to the size distribution of $(Au\text{-}10)_{0.50}$ and $(Ag\text{-}10)_{0.50}$ colloids. The reduction in the size distribution in bimetallic colloids is due to their tendency to form the alloy, in accordance with the previously reported results [50]. The formation of the bimetallic Au–Ag alloy was also reflected in XRD diffractograms (Figure 6) and UV–VIS spectroscopic studies (Figure 8). A reduction in the size distribution of dextran-stabilized Ag–Au bimetallic alloy NPs as compared to dextran-stabilized Ag-NPs was also observed in previous research [50]. This reduction in the size distribution in bimetallic alloy colloids definitely has a viable impact on their interaction with the biological system [51].

### *3.5. Antiviral Activities*

After the comprehensive characterization of various synthesized metallic and bimetallic gold and silver nanostructures with XRD, SEM, UV–VIS and DLS, we investigated their antiviral activities against the Avian Influenza H9N2 virus strain. The hemagglutination assay test has been used to detect the presence of a typical virus on the basis of its hemagglutination ability. H9N2 influenza A virus has the ability to agglutinate chicken Red Blood Cells (RBCs). Perusing the procedure referenced by Alexander and Chettle, the competing viral property of H9N2 influenza A virus for agglutinating chicken Red Blood Cells (RBCs)

and the gold and silver nanostructures' antiviral property of disabling virus activity have been examined. [52]. The detailed procedure is described in Section 2.3. It is also seen in the literature that bimetallic gold–silver nanostructures have synergistically improved their antibacterial activities, as compared to monometallic counterparts, against various microbes [24,25]. In this section, an attempt has been made to investigate the antiviral tendency of bimetallic gold–silver nanostructures and their monometallic counterparts synthesized by the atmospheric pressure microplasma technique. The Haemagglutinin Activity (HA) of AIV/H9N2 after the interaction with different concentrations of $(Au\text{-}10)_{0.50}$, $(Ag\text{-}10)_{0.50}$ and $(Au–Ag\text{-}10)_{0.50}$ colloids fabricated by an atmospheric pressure microplasma discharge of 10 min in micro titration is shown in Figures 10–12. The concentration of the nanostructures in the precursor composition that can inhibit the virus activity has been evaluated by using the standard relation [53].

$$\text{Mass} = \text{Molarity} \times \text{Molecular Wight} \times \text{volume} \quad (2)$$

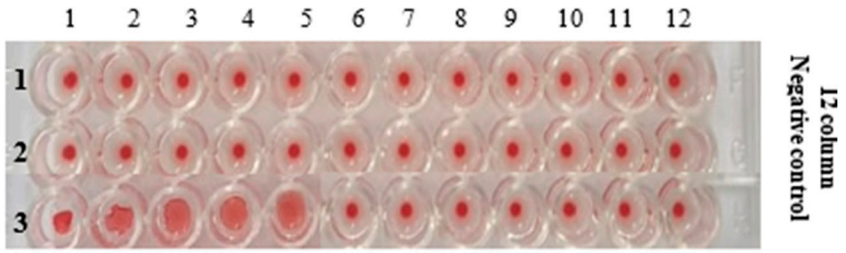


**Figure 10.** U-bottom micro titration plate showing the HA activity of AIV/H9N2 after mixing with different concentrations of $(Au\text{-}10)_{0.50}$ (gold colloids).

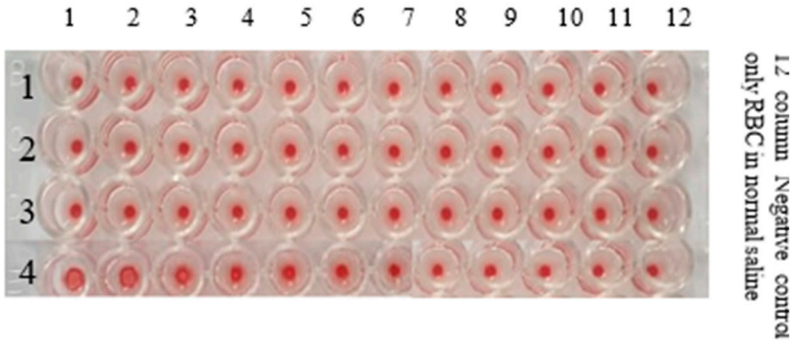


**Figure 11.** U-bottom micro titration plate showing the HA Activity of AIV/H9N2 after mixing with different concentrations of $(Ag\text{-}10)_{0.50}$ (Silver Colloids).

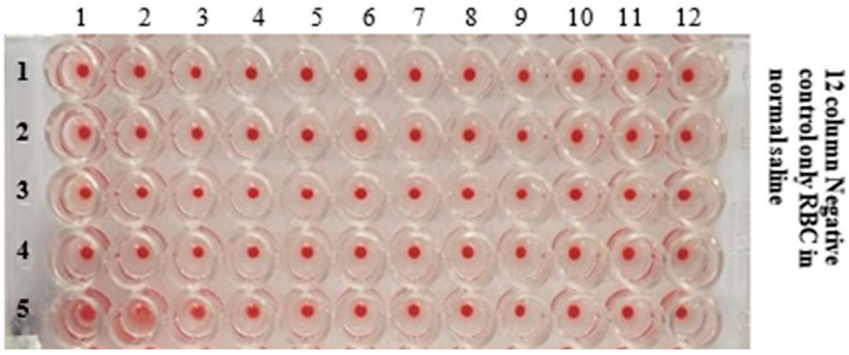


**Figure 12.** U-bottom micro well plate showing the HA Activity of AIV/H9N2 after mixing with different concentrations of $(Au–Ag\text{-}10)_{0.50}$ gold-silver bimetallic colloids.

#### 3.5.1. HA Activity of AIV/H9N2 after the Interaction with $(Au\text{-}10)_{0.50}$

The HA activity of AIV/H9N2 in the presence of the different concentrations of gold colloids was reduced from 0.5 mM $HAuCl_4 \cdot 3H_2O$ by 10 min of microplasma discharge exposure, which has been investigated in this section. With the twofold serial dilutions, the confirmed concentration of $(Au\text{-}10)_{0.50}$ that can attenuate the AIV/H9N2 activity has been evaluated to be 4.9 µg/mL. However, at the concentration of 2.45 µg/mL, the HA activity was positive, as shown in Figure 10. Table 2 gives the details of the Haemegglutination Assay protocols for studying the inhibiting tendency of gold colloids.

**Table 2.** HA Activity of AIV/H9N2 After Mixing with Different Concentrations of the $(Au\text{-}10)_{0.50}$ (Gold Nanostructures) Formulation by 10 min of Microplasma Discharge Time.

| Sample ID/Au-10 | Precursor Concentration ($HAuCl_4 \cdot 3H_2O$) | Concentration of Nanostructure Gold | HA Activity |
|---|---|---|---|
| 1 | 0.50 mM | 9.8 µg/mL | −Ve |
| 2 | 0.25 mM | 4.9 µg/mL | −Ve |
| 3 | 0.125 mM | 2.45 µg/mL | +Ve |

#### 3.5.2. HA Activity of AIV/H9N2 after the Interaction with $(Ag\text{-}10)_{0.50}$ (Silver Colloids)

The Haemagglutinin Activity (HA) of AIV/H9N2 after the interaction with different concentrations of $(Ag\text{-}10)_{0.50}$ colloids fabricated by an atmospheric pressure microplasma discharge of 10 min in micro titration is shown in Figure 11. The details of the HA activity of AIV/H9N2 in the presence of the different concentrations of silver $(Ag\text{-}10)_{0.50}$ nanoparticles are depicted in Table 2. The confirmed concentration of silver nanostructures that could disable the AIV/H9N2 virus activity has been observed to be 13.4 µg/mL, while at 5.39 µg/mL, the HA activity was positive, as evidenced in Figure 11.

#### 3.5.3. HA Activity of AIV/H9N2 after the Interaction with $(Au–Ag\text{-}10)_{0.50}$ (Gold–Silver Bimetallic Colloids)

The Haemagglutinin Activity (HA) of AIV/H9N2 after the interaction with different concentrations of $(Au–Ag\text{-}10)_{0.50}$ colloids fabricated by an atmospheric pressure microplasma discharge of 10 min in micro titration is shown in Figure 12. Moreover, the detailed antiviral activity of gold–silver bimetallic colloids is presented in Table 3, where it can be observed that gold–silver colloids can attenuate the infectivity of H9N2 influenza virus with a concentration of 3.18 µg/mL.

**Table 3.** HA Activity of AIV/H9N2 after Mixing with Different Concentrations of Silver NPs Formulation by 10 min of Microplasma Discharge Time.

| Sample $(Ag\text{-}10)_{0.50}$ | Precursor ($AgNO_3$) Concentration | Concentration of Nanostructured Silver Particles | HA Activity |
|---|---|---|---|
| 1 | 0.5 mM | 53.9 µg/mL | −Ve |
| 2 | 0.25 mM | 26.9 µg/mL | −Ve |
| 3 | 0.125 mM | 13.4 µg/mL | −Ve |
| 4 | 0.05 mM | 5.39 µg/mL | +Ve |

The HA activity of AIV/H9N2 interaction with different concentrations of gold, silver and gold–silver colloids is shown in micro titration plates in Figures 10–12, respectively. The concentrations of gold, silver and gold–silver nanostructures for counteracting AIV/H9N2 have been recorded in Tables 2–4, respectively, computed by the standard relation [53]. With the two-fold serial dilution, it is observed that the confirmed concentration of $(Au\text{-}10)_{0.50}$ gold colloids that can inhibit AIV/H9N2 activity is 4.9 µg/mL, as depicted in Figure 10 and Table 2. This is quite satisfactory compared to the recently investigated antiviral activity of porous-gold NPs prepared by a surfactant-free emulsion method against the H1N1, H3N2 and H9N2 influenza virus strains in the HA protocol using Madin–Darby Canine Kidney

(MDCK) cells as a culture medium [14]. Their observations yielded 0.2 mg/mL for the minimum concentration of porous AuNPs needed to inactivate the effects of these virus strains. The confirmed concentration of Silver colloids that could disable the AIV/H9N2 virus activity was observed to be 13.4 µg/mL, as illustrated in Figure 11 and Table 3. In a similar kind of past study, the silver nanoparticles prepared by the green synthesis method had shown a potential tendency of inhibiting H1N1 influenza A virus activity with a concentration range of 12.5 µg/mL to 100 µg/mL [54]. In the present study, the confirmed concentration of silver nanoparticles prepared by the microplasma technique that can inhibit H9N2 Influenza A virus activity lies within this range.

**Table 4.** HA Activity of AIV/H9N2 After Mixing with Different Concentrations of $(Au–Ag\text{-}10)_{0.50}$.

| Sample/ $(Au–Ag\text{-}10)_{0.50}$ | Precursor Concentration (0.25 mM $HAuCl_4 \cdot 3H_2O$ + 0.25 mM $AgNO_3$) | Concentration of $(Au–Ag\text{-}10)_{0.50}$ | HA Activity |
|---|---|---|---|
| 1 | 0.50 mM | 31.8 µg/mL | −Ve |
| 2 | 0.25 mM | 15.9 µg/mL | −Ve |
| 3 | 0.125 mM | 7.95 µg/mL | −Ve |
| 4 | 0.05 mM | 3.18 µg/mL | −Ve |
| 5 | 0.025 mM | 1.59 µg/mL | +Ve |

Moreover, the detailed antiviral activity of gold–silver bimetallic colloids is presented in Table 4. The confirmed concentration of gold–silver bimetallic colloids that could disable the AIV/H9N2 virus activity was observed to be 3.18 µg/mL, as shown in Figure 12. From the present observations, it is seen that $(Au\text{-}10)_{0.50}$, $(Ag\text{-}10)_{0.50}$ and $(Au–Ag\text{-}10)_{0.50}$ bimetallic NPs with crystalline nanostructures, as evidenced in the XRD analysis [30], remarkably inhibited the influenza virus H9N2 activity. One strong reason for such a convincing antiviral efficiency is assumed to be the compatibility of the size range of microplasma-fabricated gold and silver colloids, as seen in our DLS analyses (in Section 3.4), which range from 55 nm to 143 nm. The avian influenza virus belonging to the orthomyxoviruses family can exist with different morphologies in the size range of 80–300 nm [55]. These compatibilities are assumed to be responsible for the effective bio-conjunction with influenza viruses [56]. Consequently, these nanostructures attach to the viral envelope glycoproteins and, hence, inhibit the virus surface activity [57]. Recently, our group found the gold–PVP hybrid nanostructure to be more effective in inhibiting the influenza H9N2 virus activity as compared bare gold particles [27].

Most importantly, in our present investigations, $(Au–Ag\text{-}10)_{0.50}$ showed a greater efficiency of inhibition against H9N2 virus activity as compared to $(Au\text{-}10)_{0.50}$ and $(Ag\text{-}10)_{0.50}$. The enhancing inhibiting capability of $(Au–Ag\text{-}10)_{0.50}$ bimetallic NPs against avian influenza is attributed to their alloy formation. The formation of $(Au–Ag\text{-}10)_{0.50}$ bimetallic alloy NPs is well supported by XRD analyses (Section 3.1), where a decrease in the peak intensities of Au–Ag (111) and Au–Ag (200) as compared to those of Au (111) and (200) is due to the formation of Au–Ag alloys [35]. The appearance of a single SPR peak in the UV–VIS spectrum of $(Au–Ag\text{-}10)_{0.50}$ NPs and its existence between the SPR peaks of $(Ag\text{-}10)_{0.50}$ colloids and $(Au\text{-}10)_{0.50}$ colloids also justify the formation of $(Au–Ag\text{-}10)_{0.50}$ bimetallic NPs in the alloy [46,58].

Another reason for the greater antiviral proficiency of $(Au–Ag\text{-}10)_{0.50}$ as compared to that of $(Au\text{-}10)_{0.50}$ NPs is the decrease in the size distribution of $(Au–Ag\text{-}10)_{0.50}$ colloids (in DLS studies; Section 3.4) in bimetallic form, which is also evidenced in UV–VIS spectroscopy (Section 3.3). This decrease in the size of $(Au–Ag\text{-}10)_{0.50}$ bimetallic alloy nanoparticles increases the effective surface area of the nanostructured particles [47]. The small particle size with an enhanced surface area causes an improvement in the surface reactivity of NPs, with the virus envelope glycoprotein favoring an enhanced antiviral activity in bimetallic alloy form [51]. Fortunately, $(Au–Ag\text{-}10)_{0.50}$ nanoparticles are fertile in compatibility due to the inherited character of the gold constituent [59], are more antimicrobial due to

the inherited character of silver NPs [60] and have a more stable character due to their existence in the alloy form [61]. Consequently, $(Au–Ag\text{-}10)_{0.50}$ alloy NPs have shown a great potential to execute an excellent surface functionalization with the influenza virus glycoprotein, disabling the hemagglutinin and neuraminidase activities of the binding host cells, resulting in synergy in the antiviral activity, as compared to its counterparts. These observations have emphasized the importance of bimetallic alloy NPs in therapeutic applications [62].

It seems pertinent to mention that, with the administration of our reported confirmed concentration of fructose-stabilized nanostructures in inhibiting AIVH9N2 virus activity, cytotoxic effects are assumed to be negligible. Our claim is strengthened by the previously reported antimicrobial potencies of starch-stabilized AuNPs and Au/Ag alloy NPs, where, up to 20 ug/mL, the cytotoxic effects of AuNPs and Au/Ag alloy NPs against healthy cells were insignificant [26]. However, these studies can be extended in the future to investigate the cytotoxic effects of microplasma-fabricated nanostructures.

## 4. Conclusions

Atmospheric pressure microplasma-assisted fabrication resulted in gold, silver and gold–silver crystalline nanostructures. An adequate change in the morphology of gold–silver bimetallic NPs has been revealed as compared to the morphology of fructose-stabilized gold particles and silver NPs. The majority of the gold–silver particles are spherical and are uniformly dispersed. Gold–silver colloids depict the bimetallic nanostructures in an alloy form. The compatibility in the sizes of both fabricated nanoparticles and the influenza virus belonging to the orthomyxoviruses family are assumed to be responsible for an effective bio-conjunction with influenza viruses. These nanostructures have demonstrated convincing antiviral activity against the Avian Influenza H9N2 virus. However, gold–silver alloy nanoparticles have synergistically improved the antiviral activity against Avian Influenza virus H9N2 as compared to the antiviral activities of their counterparts. It is conclusively stated that bimetallic nanocomposites could be better antiviral options to control and hence to eradicate the viral diseases. In the future, this research work can be extended to design an atmospheric pressure microplasma setup to fabricate metallic oxide nanocomposites of copper, Fe and Zn on a large scale. Moreover, these studies can be further extended to investigate the antiviral activates against other enveloped viruses such as Hepatitis C virus (HCV) and human coronaviruses (SARS-CoV-2). Furthermore, the cytotoxic effects of microplasma-fabricated nanostructures can also be explored in future works.

**Author Contributions:** Conceptualization, M.Z.; methodology, M.Z.; software, A.K.; validation, A.K., M.S.R. and T.Y. formal analysis, M.A.S.; investigation, M.Z.; resources, T.Y.; data curation, M.F.S.; writing—original draft preparation, M.Z.; writing—review and editing, M.Z.; visualization, M.S.R.; supervision, M.S.R. and T.Y.; funding acquisition, S.Y.A. All authors have read and agreed to the published version of the manuscript.

**Funding:** The authors would like to thank the Researchers Supporting Project Number (RSP2023R35), King Saud University, Riyadh, Saudi Arabia.

**Data Availability Statement:** It is hereby stated that all the experimental manipulations concerning the project entitled 'The fabrication of gold–silver bimetallic colloids by microplasma: A worthwhile strategy for counteracting the surface activity of avian influenza virus' are undertaken in compliance with the institutional guidelines of Ethical Review committee, Institute of Microbiology, University of Veterinary and Animal Sciences Lahore. The documentation of compliance with the ethical standard from the concerned authorities may be provided on acceptance of the manuscript.

**Acknowledgments:** The authors would like to thank the Researchers Supporting Project Number, (RSP2023R35), King Saud University, Riyadh, Saudi Arabia.

**Conflicts of Interest:** It is hereby stated that there have been no competing interest associated with this research work from the start of the research, during the research and after its completion. It is further declared that the authors have no relevant financial or non-financial interests to disclose. It is further declared that no funds, grants or financial support were received during the preparation of this manuscript. It is confirmed that the manuscript has been read and approved by all of the named authors and that there are no other persons who satisfy the criteria for authorship but are not mentioned.

## References


1. Peacock, T.P.; James, J.; Sealy, J.E.; Iqbal, M. A global perspective on $H_9N_2$ avian influenza virus. *Viruses* **2019**, *11*, 620. [CrossRef] [PubMed]
2. Gillim-Ross, L.; Subbarao, K. Emerging respiratory viruses: Challenges and vaccine strategies. *Clin. Microbiol. Rev.* **2006**, *19*, 614–636. [CrossRef] [PubMed]
3. Alexander, M.E.; Bowman, C.S.; Feng, Z.; Gardam, M.; Moghadas, S.M.; Röst, G.; Wu, J.; Yan, P. Emergence of drug resistance: Implications for antiviral control of pandemic influenza. *Proc. R. Soc. B Boil. Sci.* **2007**, *274*, 1675–1684. [CrossRef] [PubMed]
4. Sun, D.; Shahzad, M.B.; Li, M.; Wang, G.; Xu, D. Antimicrobial materials with medical applications. *Mater. Technol.* **2014**, *30*, B90–B95. [CrossRef]
5. Nasrollahzadeh, M.; Sajadi, S.M.; Sajjadi, M.; Issaabadi, Z. Applications of nanotechnology in daily life. *Interface Sci. Technol.* **2019**, *28*, 113–143. [CrossRef]
6. Yah, C.S.; Simate, G.S. Nanoparticles as potential new generation broad spectrum antimicrobial agents. *DARU J. Pharm. Sci.* **2015**, *23*, 43. [CrossRef]
7. Wang, L.; Hu, C.; Shao, L. The antimicrobial activity of nanoparticles: Present situation and prospects for the future. *Int. J. Nanomed.* **2017**, *12*, 1227–1249. [CrossRef]
8. Senarathna, U.; Fernando, S.S.N.; Gunasekara, T.D.C.P.; Weerasekera, M.M.; Hewageegana, H.G.S.P.; Arachchi, N.D.H.; Siriwardena, H.D.; Jayaweera, P.M. Enhanced antibacterial activity of $TiO_2$ nanoparticle surface modified with Garcinia zeylanica extract. *Chem. Central J.* **2017**, *11*, 1–8. [CrossRef]
9. Sirelkhatim, A.; Mahmud, S.; Seeni, A.; Kaus, N.H.M.; Ann, L.C.; Bakhori, S.K.M.; Hasan, H.; Mohamad, D. Review on zinc oxide nanoparticles: Antibacterial activity and toxicity mechanism. *Nano-Micro Lett.* **2015**, *7*, 219–242. [CrossRef]
10. Mansoureh, G.; Parisa, V. Synthesis of Metal Nanoparticles Using Laser Ablation Technique. In *Emerging Applications of Nanoparticles and Architecture Nanostructures*; Elsevier: Amsterdam, The Netherlands, 2018; pp. 575–596.
11. Kumar, H.; Venkatesh, N.; Bhowmik, H.; Kuila, A. Metallic nanoparticle: A review. *Biomed. J. Sci. Tech. Res.* **2018**, *4*, 3765–3775.
12. Sametband, M.; Shukla, S.; Meningher, T.; Hirsh, S.; Mendelson, E.; Sarid, R.; Gedanken, A.; Mandelboim, M. Effective multi-strain inhibition of influenza virus by anionic gold nanoparticles. *Med. Chem. Comm.* **2011**, *2*, 421–423. [CrossRef]
13. Mehrbod, P.; Motamed, N.; Tabatabaeian, M.; Soleymani, E.R.; Amini, E.; Shahidi, M.; Kheyri, M.T. In Vitro Antiviral Effect of."Nanosilver" on influenza virus. *DARU* **2009**, *17*, 88–93.
14. Kim, J.; Yeom, M.; Lee, T.; Kim, H.-O.; Na, W.; Kang, A.; Lim, J.-W.; Park, G.; Park, C.; Song, D.; et al. Porous gold nanoparticles for attenuating infectivity of influenza A virus. *J. Nanobiotechnol.* **2020**, *18*, 54. [CrossRef] [PubMed]
15. Bhattacharya, C.; Jagirdar, B.R. Monodisperse colloidal metal nanoparticles to core–shell structures and alloy nanosystems via digestive ripening in conjunction with solvated metal atom dispersion: A mechanistic study. *J. Phys. Chem. C* **2018**, *122*, 10559–10574. [CrossRef]
16. Chang, S.Y.; Huang, K.Y.; Chao, T.L.; Kao, H.C.; Pang, Y.H.; Lu, L.; Chiu, L.; Huang, C.; Cheng, J.R.; Fang, M.; et al. Nanoparticle composite TPNT1 is effective against SARS-CoV-2 and influenza viruses. *Sci. Rep.* **2021**, *11*, 1–13. [CrossRef] [PubMed]
17. Yadavalli, T.; Shukla, D. Role of metal and metal oxide nanoparticles as diagnostic and therapeutic tools for highly prevalent viral infections. *Nanomed. Nanotechnol. Biol. Med.* **2016**, *13*, 219–230. [CrossRef]
18. Yallappa, S.; Manjanna, J.; Dhananjaya, B. Phytosynthesis of stable Au, Ag and Au–Ag alloy nanoparticles using J. Sambac leaves extract, and their enhanced antimicrobial activity in presence of organic antimicrobials. *Spectrochim. Acta Part A Mol. Biomol. Spectrosc.* **2015**, *137*, 236–243. [CrossRef]
19. Pham, T.T.H.; Dien, N.D.; Vu, X.H. Facile synthesis of silver/gold alloy nanoparticles for ultra-sensitive rhodamine B detection. *RSC Adv.* **2021**, *11*, 21475–21488. [CrossRef]
20. Ferrando, R.; Jellinek, J.; Johnston, R.L. Nanoalloys: From Theory to Applications of Alloy Clusters and Nanoparticles. *Chem. Rev.* **2008**, *108*, 845–910. [CrossRef]
21. Pal, A.; Shah, S.; Devi, S. Preparation of Silver—Gold Alloy Nanoparticles at Higher Concentration Using Sodium Dodecyl Sulfate. *Aust. J. Chem.* **2008**, *61*, 66–71. [CrossRef]
22. Banerjee, M.; Sharma, S.; Chattopadhyay, A.; Ghosh, S.S. Enhanced antibacterial activity of bimetallic gold-silver core–shell nanoparticles at low silver concentration. *Nanoscale* **2011**, *3*, 5120–5125. [CrossRef] [PubMed]
23. Ramasamy, M.; Lee, J.-H.; Lee, J. Potent antimicrobial and antibiofilm activities of bacteriogenically synthesized gold–silver nanoparticles against pathogenic bacteria and their physiochemical characterizations. *J. Biomater. Appl.* **2016**, *31*, 366–378. [CrossRef] [PubMed]

24. Nazeruddin, G.M.; Prasad, R.N.; Shaikh, Y.I.; Shaikh, A.A. Synergetic effect of Ag–Cu bimetallic nanoparticles on antimicrobial activity. *Der Pharm. Lett.* **2014**, *3*, 129–136.
25. Perdikaki, A.; Galeou, A.; Pilatos, G.; Karatasios, I.; Kanellopoulos, N.K.; Prombona, A.; Karanikolos, G.N. Ag and Cu Monometallic and Ag/Cu Bimetallic Nanoparticle–Graphene Composites with Enhanced Antibacterial Performance. *ACS Appl. Mater. Interfaces* **2016**, *8*, 27498–27510. [CrossRef]
26. Lomelí-Marroquín, D.; Cruz, D.M.; Nieto-Argüello, A.; Crua, A.V.; Chen, J.; Torres-Castro, A.; Webster, T.J.; Cholula-Díaz, J.L. Starch-mediated synthesis of mono- and bimetallic silver/gold nanoparticles as antimicrobial and anticancer agents. *Int. J. Nanomed.* **2019**, *14*, 2171. [CrossRef]
27. Zubair, M.; Rafique, M.S.; Khalid, A.; Yaqub, T.; Alomar, S.Y.; Gohar, H. Synthesis of Gold-PVP Nanostructured Composites by Microplasma: A Test to Study Their Inhibiting Tendency of Avian Influenza Virus Activity. *Appl. Sci.* **2022**, *12*, 5352. [CrossRef]
28. Mariotti, D.; Sankaran, R.M. Microplasmas for nanomaterials synthesis. *J. Phys. D Appl. Phys.* **2010**, *43*, 323001. [CrossRef]
29. Khatoon, N.; Yasin, H.M.; Younus, M.; Ahmed, W.; Rehman, N.U.; Zakaullah, M.; Iqbal, M.Z. Synthesis and spectroscopic characterization of gold nanoparticles via plasma-liquid interaction technique. *AIP Adv.* **2018**, *8*, 015130. [CrossRef]
30. Kaneko, T.; Baba, K.; Harada, T.; Hatakeyama, R. Novel gas-liquid interfacial plasmas for synthesis of metal nanoparticles. *Plasma Process. Polym.* **2009**, *6*, 713–718. [CrossRef]
31. Wang, R.; Zuo, S.; Wu, D.; Zhang, J.; Zhu, W.; Becker, K.H.; Fang, J. Microplasma-assisted synthesis of colloidal gold nanoparticles and their use in the detection of cardiac troponin I (cTn-I). *Plasma Process. Polym.* **2014**, *12*, 380–391. [CrossRef]
32. McKenna, J.; Patel, J.; Mitra, S.; Soin, N.; Svrcek, V.; Maguire, P.; Mariotti, D. Synthesis and surface engineering of nanomaterials by atmospheric-pressure microplasmas. *Eur. Phys. J. Appl. Phys.* **2011**, *56*, 24020. [CrossRef]
33. Zhang, G.; Du, M.; Li, Q.; Li, X.; Huang, J.; Jiang, X.; Sun, D. Green synthesis of Au–Ag alloy nanoparticles using Cacumen platycladi extract. *RSC Adv.* **2012**, *3*, 1878–1884. [CrossRef]
34. Dhoondia, Z.H.; Chakraborty, H. *Lactobacillus* Mediated Synthesis of Silver Oxide Nanoparticles. *Nanomater. Nanotechnol.* **2012**, *2*, 15. [CrossRef]
35. Bharati, M.S.S.; Byram, C.; Soma, V.R. Femtosecond laser fabricated Ag@Au and Cu@au alloy nanoparticles for surface enhanced raman spectroscopy based trace explosives detection. *Front. Phys.* **2018**, *6*, 28. [CrossRef]
36. Basavaraja, S.; Balaji, S.D.; Lagashetty, A.; Rajasab, A.H.; Venkataraman, A. Extracellular biosynthesis of silver nanoparticles using the fungus Fusarium semitectum. *Mater. Res. Bull.* **2008**, *43*, 1164–1170. [CrossRef]
37. Wang, A.; Hsieh, Y.-P.; Chen, Y.-F.; Mou, C.-Y. Au–Ag alloy nanoparticle as catalyst for CO oxidation: Effect of Si/Al ratio of mesoporous support. *J. Catal.* **2005**, *237*, 197–206. [CrossRef]
38. Patterson, A.L. The Scherrer Formula for X-Ray Particle Size Determination. *Phys. Rev.* **1939**, *56*, 978–982. [CrossRef]
39. Liu, J.; Zangeneh, A.; Zangeneh, M.M.; Guo, B. Antioxidant, cytotoxicity, anti-human esophageal squamous cell carcinoma, anti-human Caucasian esophageal carcinoma, anti-adenocarcinoma of the gastroesophageal junction, and anti-distal esophageal adenocarcinoma properties of gold nanoparticles green synthesized by Rhus coriaria L. fruit aqueous extract. *J. Exp. Nanosci.* **2020**, *15*, 202–216. [CrossRef]
40. Kolenčík, M.; Ernst, D.; Komár, M.; Urík, M.; Šebesta, M.; Ďurišová, L.; Bujdoš, M.; Černý, I.; Chlpík, J.; Juriga, M.; et al. Effects of Foliar Application of ZnO Nanoparticles on Lentil Production, Stress Level and Nutritional Seed Quality under Field Conditions. *Nanomaterials* **2022**, *12*, 310. [CrossRef]
41. Singh, R. Navneet Green synthesis of silver nanoparticles using methanol extract of Ipomoea carnea Jacq to combat multidrug resistance bacterial pathogens. *Curr. Res. Green Sustain. Chem.* **2021**, *4*, 100152. [CrossRef]
42. Iqbal, T.; Mukhtar, M.; Khan, M.A.; Khan, R.; Zaman, R.; Mahmood, H.; Zaka-Ul-Islam, M. Atmospheric pressure microplasma assisted growth of silver nanosheets and their inhibitory action against bacteria of clinical interest. *Mater. Res. Express* **2016**, *3*, 125019. [CrossRef]
43. Kumar, S.; Majhi, R.K.; Singh, A.; Mishra, M.; Tiwari, A.; Chawla, S.; Guha, P.; Satpati, B.; Mohapatra, H.; Goswami, L.; et al. Carbohydrate-Coated Gold–Silver Nanoparticles for Efficient Elimination of Multidrug Resistant Bacteria and in Vivo Wound Healing. *ACS Appl. Mater. Interfaces* **2019**, *11*, 42998–43017. [CrossRef] [PubMed]
44. Al-Haddad, J.; Alzaabi, F.; Pal, P.; Rambabu, K.; Banat, F. Green synthesis of bimetallic copper–silver nanoparticles and their application in catalytic and antibacterial activities. *Clean Technol. Environ. Policy* **2019**, *22*, 269–277. [CrossRef]
45. William, R.V.; Das, G.M.; Dantham, V.R.; Laha, R. Enhancement of single molecule raman scattering using sprouted potato shaped bimetallic nanoparticles. *Sci. Rep.* **2019**, *9*, 10771. [CrossRef]
46. Diem, P.N.H.; Phuong, T.N.M.; Hien, N.Q.; Quang, D.T.; Hoa, T.T.; Cuong, N.D. Silver, gold, and silver-gold bimetallic nanoparticle-decorated dextran: Facile synthesis and versatile tunability on the antimicrobial activity. *J. Nanomater.* **2020**, *2020*, 7195048. [CrossRef]
47. Baranwal, A.; Srivastava, A.; Kumar, P.; Bajpai, V.K.; Maurya, P.K.; Chandra, P. Prospects of Nanostructure Materials and Their Composites as Antimicrobial Agents. *Front. Microbiol.* **2018**, *9*, 422. [CrossRef]
48. Chen, Y.-H.; Yeh, C.-S. A new approach for the formation of alloy nanoparticles: Laser synthesis of gold–silver alloy from gold–silver colloidal mixturesElectronic supplementary information (ESI) available: Experimental details, UV–VIS spectra, TEM images and EDX analysis for molar ratios (Au:Ag) of 1:2 and 2:1. See http://www.rsc.org/suppdata/cc/b0/b009854j. *Chem. Commun.* **2001**, *4*, 371–372.

49. Liu, H.; Pierre-Pierre, N.; Huo, Q. Dynamic light scattering for gold nanorod size characterization and study of nanorod–protein interactions. *Gold Bull.* **2012**, *45*, 187–195. [CrossRef]
50. Bankura, K.; Maity, D.; Mollick, M.R.; Mondal, D.; Bhowmick, B.; Roy, I.; Midya, T.; Sarkar, J.; Rana, D.; Acharya, K.; et al. Antibacterial activity of Ag–Au alloy NPs and chemical sensor property of Au NPs synthesized by dextran. *Carbohydr. Polym.* **2014**, *107*, 151–157. [CrossRef]
51. Tabrizi, N.S.; Tazikeh, M.; Shahgholi, N. Antibacterial Properties of Au-Ag Alloy Nanoparticles. *Int. J. Green Nanotechnol.* **2012**, *4*, 489–494. [CrossRef]
52. Alexander, D.; Chettle, N. Procedures for the haemagglutination and the haemagglutination inhibition tests for avian infectious bronchitis virus. *Avian Pathol.* **1977**, *6*, 9–17. [CrossRef] [PubMed]
53. Andrews, J.M. Determination of minimum inhibitory concentrations. *J. Antimicrob. Chemother.* **2001**, *48* (Suppl. 1), 5–16. [CrossRef] [PubMed]
54. Xiang, D.-X.; Chen, Q.; Pang, L.; Zheng, C.-L. Inhibitory effects of silver nanoparticles on H1N1 influenza A virus in vitro. *J. Virol. Methods* **2011**, *178*, 137–142. [CrossRef] [PubMed]
55. King, A.M.; Lefkowitz, E.; Adams, M.J.; Carstens, E.B. (Eds.) Family Orthomyxoviridae. In *Virus Taxonomy: Ninth Report of the International Committee on Taxonomy of Viruses*; Elsevier: Amsterdam, The Netherlands, 2012; pp. 749–761.
56. Singh, L.; Kruger, H.G.; Maguire, G.; Govender, T.; Parboosing, R. The role of nanotechnology in the treatment of viral infections. *Ther. Adv. Infect. Dis.* **2017**, *4*, 105–131. [CrossRef]
57. Paradowska, E.; Studzińska, M.; Jabłońska, A.; Lozovski, V.; Rusinchuk, N.; Mukha, I.; Vitiuk, N.; Leśnikowski, Z.J. Antiviral Effect of Nonfunctionalized Gold Nanoparticles against Herpes Simplex Virus Type-1 (HSV-1) and Possible Contribution of Near-Field Interaction Mechanism. *Molecules* **2021**, *26*, 5960. [CrossRef]
58. Moskovits, M.; Srnová-Šloufová, I.; Vlčková, B. Bimetallic Ag–Au nanoparticles: Extracting meaningful optical constants from the surface-plasmon extinction spectrum. *J. Chem. Phys.* **2002**, *116*, 10435–10446. [CrossRef]
59. Parida, U.K.; Biswal, S.K.; Nayak, P.L.; Bindhani, B.K. Gold nano particles for biomedical applications. *World J. Nano Sci. Technol.* **2013**, *2*, 47–57.
60. Crisan, C.M.; Mocan, T.; Manolea, M.; Lasca, L.I.; Tăbăran, F.-A.; Mocan, L. Review on silver nanoparticles as a novel class of antibacterial solutions. *Appl. Sci.* **2021**, *11*, 1120. [CrossRef]
61. Soenen, S.J.; Parak, W.J.; Rejman, J.; Manshian, B. (Intra) cellular stability of inorganic nanoparticles: Effects on cytotoxicity, particle functionality, and biomedical applications. *Chem. Rev.* **2015**, *115*, 2109–2135. [CrossRef]
62. Hu, X.; Xu, X.; Fu, F.; Yang, B.; Zhang, J.; Zhang, Y.; Touhid, S.S.B.; Liu, L.; Dong, Y.; Liu, X.; et al. Synthesis of bimetallic silver-gold nanoparticle composites using a cellulose dope: Tunable nanostructure and its biological activity. *Carbohydr. Polym.* **2020**, *248*, 116777. [CrossRef]